Journal of Alloys and Compounds 589 (2014) 218–225

Contents lists available at ScienceDirect

Journal of Alloys and Compounds

journal homepage: www.elsevier.com/locate/jalcom

Photovoltaic performance enhancement of CdS quantum dot-sensitized TiO_2 photoanodes with plasmonic gold nanoparticles

Aiping Liu [a,b,*], Qinghua Ren [a], Ming Zhao [a], Tao Xu [a], Ming Yuan [a], Tingyu Zhao [a], Weihua Tang [c]

[a] Center for Optoelectronics Materials and Devices, Zhejiang Sci-Tech University, Hangzhou 310018, China
[b] State Key Laboratory of Silicon Materials, Zhejiang University, Hangzhou 310027, China
[c] State Key Laboratory of Information Photonics and Optical Communication, Beijing University Posts and Telecommunications, Beijing 100876, China

ARTICLE INFO

Article history:
Received 13 July 2013
Received in revised form 14 November 2013
Accepted 16 November 2013
Available online 23 November 2013

Keywords:
Metallic plasmon
Quantum dot-sensitized solar cells
Photovoltaic behavior
Light scattering and concentrating

ABSTRACT

The CdS quantum dot-sensitized TiO_2 films with plasmonic gold nanoparticles were designed as photoanodes by the electrodeposition of gold combined with the "successive ionic layer adsorption and reaction" (SILAR) method for CdS deposition on porous TiO_2 films. A prominent enhancement in light absorption of Au/TiO_2/CdS hybrid was attained by efficient light scattering of gold plasmons as sub-wavelength antennas and concentrators. The photogenerated electron formed in the near-surface region of TiO_2 and CdS were facilitated to transfer to the plasmonic gold, resulting in the enhancement of photocurrent and incident photon-to-current conversion efficiency of hybrid photoanode upon photoirradiation. Furthermore, the photovoltaic response of hybrid was highly tunable with respect to the number of SILAR cycles applied to deposit CdS. The thicker absorber layer with less porous structure and larger CdS crystals might limit the electrolyte diffusion into the hybrid electrode and impose a barrier for electron tunneling and transferring. The highly versatile and tunable properties of Au/TiO_2/CdS photoanodes demonstrated their potential application in energy conversion devices.

1. Introduction

Quantum dot-sensitized solar cells (QDSSCs) are considered as a promising candidate for the development of next generation solar cells because of the simple and low-cost fabrication techniques [1–3]. Titanium dioxide (TiO_2) with a wide band gap (about 3.2 eV) is usually used as a photoanode material in the QDSSCs and photocatalysts [4,5] which absorbs the sunlight in the ultraviolet region [6]. Semiconductor QDs such as CdS [7–9], CdSe [10], PbS [11], PbSe [12] and InP [13] which absorb light in the visible or infrared regions can favor the injection of excited electrons to TiO_2 in order to improve energy conversion efficiency of QDSSCs [14,15]. However, the relatively low conversion efficiency of such cells is still a primary challenge for the large-scale application of QDSSCs.

It is well known that an effective method for enhancing light harvesting or trapping to develop high-efficiency photovoltaic devices is the mergence of metallic nanostructures with high absorption and scattering cross section [16,17]. It has been reported that metal nanoparticles (NPs), such as gold and silver, can enhance the photoresponse of photovoltaic devices by acting as photosensitizers [18], light trapping agent [19,20] and electron traps for facilitating charge separation [21,22]. The silver and gold NPs have strong absorption in the visible region due to surface plasmon resonance (SPR) effect associated with the enhancement of electromagnetic field due to collective electron oscillation [23]. For example, Liu et al. fabricated CdSe sensitized Au/TiO_2 hybrid by chemical bath deposition and observed significant enhancement in photocurrent due to the light scattering of gold NPs [24]. Nishijima et al. obtained improved photoelectric conversion in the TiO_2 single crystal via gold nanorods with localized SP effect [25]. The recent advances in control of metal plasmons synthesis and self-assembly have successfully tailored high absorption of absorber layers throughout the visible region to the near infrared one by varying metal size and shape [26,27]. Among these fabrication techniques, the electrodeposition with simple, rapid and low-cost properties can produce well-defined metallic nanostructures with SP-active nature and is regarded to be practical for mass production [28–30]. In this work, we fabricated CdS QDs sensitized porous TiO_2 film with plasmonic gold NPs to achieve Au/TiO_2/CdS hybrid films on the FTO-coated glass substrate. The gold NPs were served as the scattering elements to couple and trap the sunlight into the QDSSCs, increasing the effective absorption cross-section and optical path length inside the absorber (Fig. 1a). The gold NPs also favored the charge separation and thereby photocurrent generation (Fig. 1b). We succeeded in developing an Au/TiO_2/CdS photovoltaic material with adjustable light absorption and photovoltaic response.

* Corresponding author at: Center for Optoelectronics Materials and Devices, Zhejiang Sci-Tech University, Hangzhou 310018, China. Tel./fax: +86 571 86843468.
E-mail address: liuaiping1979@gmail.com (A. Liu).

0925-8388/$ - see front matter © 2013 Elsevier B.V. All rights reserved.
http://dx.doi.org/10.1016/j.jallcom.2013.11.106

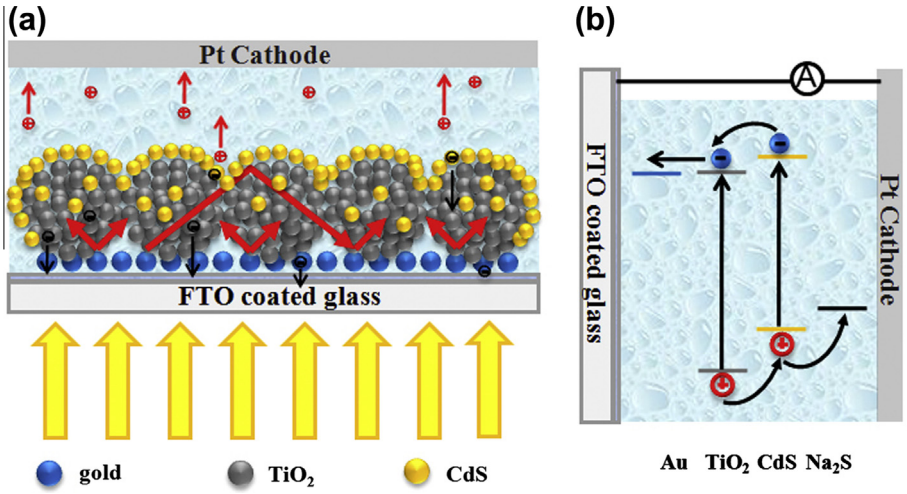

Fig. 1. (a) Schematic illustration of CdS QD-sensitized porous TiO_2 with plasmonic gold nanoparticles (NPs). The gold NPs as scatter could effectively enhance light absorption of CdS QDs as sensitizer for TiO_2 upon photoirradiation, thereby the overall photoresponse of hybrid photoanode. (b) Schematic representation of separation and transfer of electron–hole pairs in CdS QD-sensitized TiO_2 solar cell with plasmonic gold NPs.

2. Experimental

2.1. Reagents

The FTO-coated glass (resistivity of 14 Ω/□ and thickness of FTO film of 300 nm, Nippon Sheet Glass, Japan) was used as transparent conducting oxide substrate. $HAuCl_4{\cdot}3H_2O$ with a purity of 99.99% was supplied by Sigma. The TiO_2 NPs (Degussa P25) was supplied by Guangzhou HuaLiSen Trade Co. Ltd. Cadmium nitrate ($Cd(NO_3)_2$) and sodium sulfide (Na_2S) were purchased from Shanghai Chemical Reagents Co. Ltd. All other chemicals were of analytical grade and used without further purification. The water was obtained from a Millipore Q purification system (resistivity >18 MΩcm).

2.2. Synthesis of CdS QD-sensitized TiO_2 photoanodes with plasmonic gold NPs

The FTO-coated glasses were cleaned ultrasonically with soapy water, acetone, ethanol and distilled water, respectively, and dried with N_2 before use. The electrochemical experiments were performed in a three-electrode system at room temperature by an electrochemical workstation (CHI630D, Shanghai Huachen) with a FTO-coated glass, a platinum foil and a saturated calomel electrode (SCE) as the

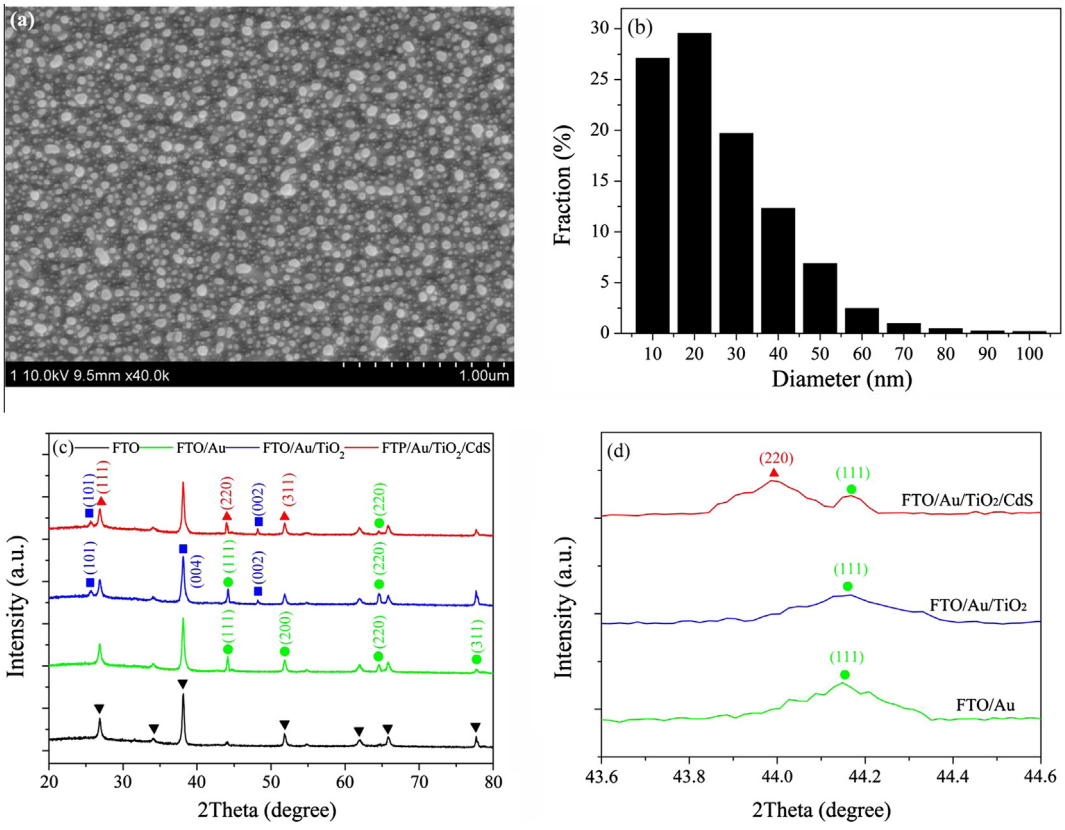

Fig. 2. (a) Scanning electron micrograph and (b) particle-size distribution of gold plasmons electrodeposited on FTO-coated glass substrates for 600 s in a 1 M Na_2SO_4 solution with $HAuCl_4$. (c) X-ray diffraction patterns of different hybrid samples. (d) Detailed X-ray diffraction patterns of different hybrid samples in the range (2θ) from 43° to 45°. The number of SILAR cycles applied to deposit CdS was 5.

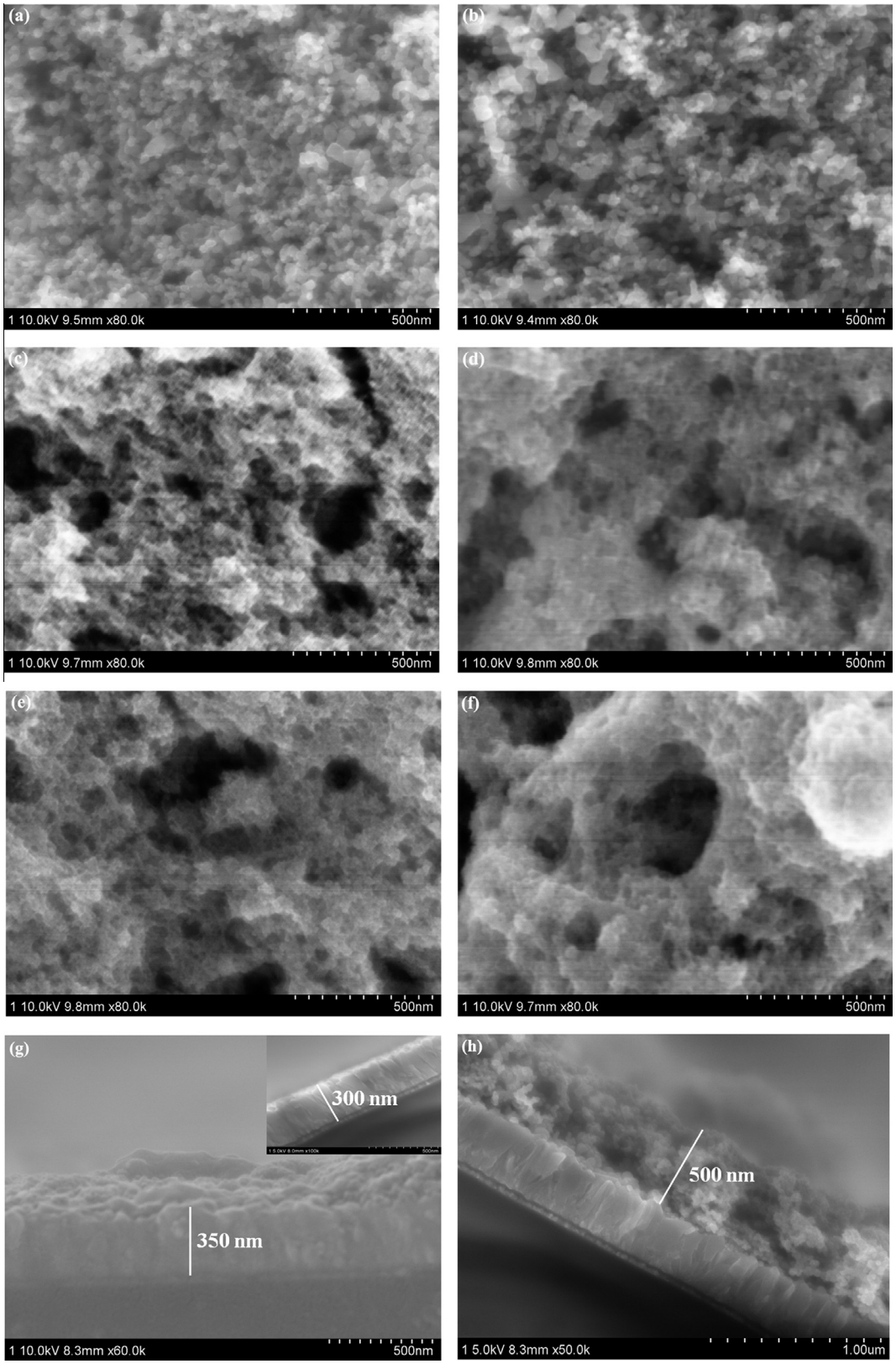

Fig. 3. Scanning electron micrographs of (a) FTO/TiO_2, (b) FTO/Au/TiO_2, (c) FTO/TiO_2/CdS, (d) FTO/Au/TiO_2/CdS, (e) FTO/TiO_2/Au/CdS and (f) FTO/Au/TiO_2/Au/CdS hybrids. The number of SILAR cycles applied to deposit CdS was 5. Cross section images of (g) FTO/TiO_2 and (h) FTO/Au/TiO_2/CdS hybrids. The inset in (g) was the corresponding cross section image of FTO-coated glass.

working, counter and reference electrodes, respectively. The FTO-coated glass was immersed into a 1 M Na_2SO_4 solution containing 0.2 mM $HAuCl_4$ to electrodeposit gold NPs on the FTO surfaces at −0.8 V (*vs.* SCE) for 600 s. The resultant FTO/Au electrodes were washed with deionized water and annealed at nitrogen atmosphere at 450 °C for 1 h. Then porous TiO_2 films were prepared by spin-coating the paste of TiO_2 NPs on the surface of FTO/Au electrodes, followed by sintering at 450 °C for 30 min in air.

The "successive ionic layer adsorption and reaction" (SILAR) method was further applied to deposit CdS QDs on the surface of TiO_2 NP films [31,32]. The cooled FTO/Au/TiO_2 electrode was dipped into a 0.5 M $Cd(NO_3)_2$ ethanol solution for 5 min, rinsed with ethanol, and then dipped into a 0.5 M Na_2S aqueous solution for another 5 min and rinsed again with water. The two-step dipping procedure was named as one SILAR cycle. Repeating the assembly cycles, the FTO/Au/TiO_2/CdS electrodes with various CdS QDs were obtained. Finally, the hybrid films were annealed at nitrogen atmosphere at 400 °C for 1 h. The FTO/TiO_2/CdS hybrids without plasmonic gold were also fabricated as the references. In order to study the effect of the position of plasmonic gold on the photovoltaic performance, the FTO/TiO_2/Au/CdS and FTO/Au/TiO_2/Au/CdS composite electrodes were also fabricated by electrodepositing gold NPs on the FTO/TiO_2 and FTO/Au/TiO_2 surfaces before CdS deposition.

2.3. Characterization and measurements

The morphologies of CdS QD-sensitized TiO_2 composite films with and without plasmonic gold NPs were characterized by a scanning electron microscopy (SEM) instrument (Hitachi S-4800, Japan). X-ray diffraction (XRD) patterns of composite films were obtained on a diffractometer (Bruker AXS D8) using the Cu Kα radiation (λ = 0.15418 nm) with a 2θ scan from 5° to 80° at a step of 0.02°. The surface area and porosity of TiO_2 films scratched off on FTO substrates were estimated by measuring the nitrogen adsorption–desorption isotherms on a Micromeritics ASAP 2020 M micropore analysis system at 77 K. The pore diameters were calculated using the Barrett–Joyner–Halenda (BJH) method. UV–vis absorption spectra of hybrid films on FTO substrates were recorded by using a UV–vis spectrophotometer (Hitachi U3900).

Photoelectrochemical performances of hybrid films were measured in a transparent quartz cell with the 0.2 M Na_2S aqueous solution as the electrolyte. The contact areas of all hybrid films were about 1.0 cm × 2.0 cm. Two-electrode system was used with the prepared hybrids as the working electrode and a platinum foil as the counter electrode. The curves of photovoltage and photocurrent versus times were recorded by the electrochemical workstation (CHI630D, Shanghai Huachen) using a 150 W Xe lamp (filtered, λ > 300 nm) as the light source. The illumination intensity near the electrode surface was about 100 mW/cm^2. Incident photon-to-current conversion efficiency (IPCE) measurements were conducted on an IPCE measurement system (Solar Cell Scan 100, Zolix) with a 150 W Xe lamp aligned into a monochromator scanning. All measurements were carried out in air at room temperature without encapsulation.

3. Results and discussion

3.1. Microstructures of CdS-sensitized TiO_2 photoanodes with plasmonic gold NPs

Fig. 2(a) shows the morphology of typical gold NPs electrodeposited on the FTO substrates, which presents a broad particle-size distribution from 10.0 nm to 95.0 nm with an average diameter about 30 nm after 600 s deposition (Fig. 2b). Fig. 2(c) shows the XRD patterns of FTO and FTO/Au samples, and the diffraction peaks appearing at (2θ) 38.0°, 44.2°, 64.6° and 77.8° are corresponding to the (111), (200), (220) and (311) planes of the face-centered cubic gold, respectively. Fig. 3 shows the morphologies of different hybrids. The TiO_2 film spin-coated on FTO-coated glass substrate shows a homogeneous porous structure with the pore diameter distribution mainly from 40 nm to 80 nm determined by using the BJH method on the desorption branch of the isotherm (Fig. 4). The TiO_2 film deposited on gold coated FTO substrate possesses an analogous porous structure (Fig. 3b) with a broader pore diameter distribution mainly from 30 nm to 85 nm (Fig. 4). The surface area also increases from 41.7 m^2/g for TiO_2 film on FTO to 48.3 m^2/g for TiO_2 film on gold coated FTO. This indicates that the gold NPs are favorable for maintaining the porous structure of TiO_2 film. When the CdS QDs are deposited on the top of TiO_2 film with and without the plasmonic gold by repeating five SILAR cycles, the FTO/TiO_2/CdS and FTO/Au/TiO_2/CdS samples remain the porous structures (Fig. 3c and d). The thicknesses of TiO_2 and CdS (five SILAR cycles) films for FTO/TiO_2/CdS and FTO/Au/TiO_2/CdS samples are about 50 nm and 450 nm since the thickness of used FTO film is about 300 nm (Fig. 3g and h). The XRD peaks at (2θ) 25.6°, 37.9° and 48.2° for TiO_2 film correspond to the (101), (004) and (200) planes of anatase phase of TiO_2 structure (Fig. 2c). The XRD peaks at (2θ) 26.6° is related to the (111) plane of cubic type of CdS structure (JCPDS No. 80-0019) (Fig. 2c). The details of the diffraction peaks from (2θ) 43.6° to 44.6° also show the signal of (220) plane of cubic type of CdS structure (Fig. 2d). In order to study the effect of gold position on the structure of composites, we fabricate the FTO/TiO_2/Au/CdS and FTO/Au/TiO_2/Au/CdS hybrids which possess larger-size porous structure (Fig. 3e and f).

3.2. Photovoltaic behaviors of CdS-sensitized TiO_2 photoanodes with plasmonic gold NPs

Fig. 5(a) shows the UV–vis absorption spectra and corresponding photographs of different samples. The FTO/Au film shows a strong absorption in the visible region between 500 nm and 600 nm due to the SPR of gold NPs. The absorption peak of plasmon mode of gold NPs on the FTO substrate is similar to that of gold NPs in an aqueous environment (centered at about 525 nm) [33,34], but with a redshift by about 30 nm due to the increase in refractive index of environment (from water to FTO-coated glass) and plasmon coupling between gold NPs [35]. The redshift of absorption peak may also be associated with the electromagnetic field enhancement around the gold NPs [26,36,37], as theoretically predicted for the localized surface plasmon resonance (LSPR) of gold [38]. Compared to the FTO/TiO_2/CdS, the significant absorption enhancement of the FTO/Au/TiO_2/CdS hybrid in the range from 500 nm to 750 nm is attributed to the action of plasmonic gold. Plasmonic-mediated absorption enhancement may be originated

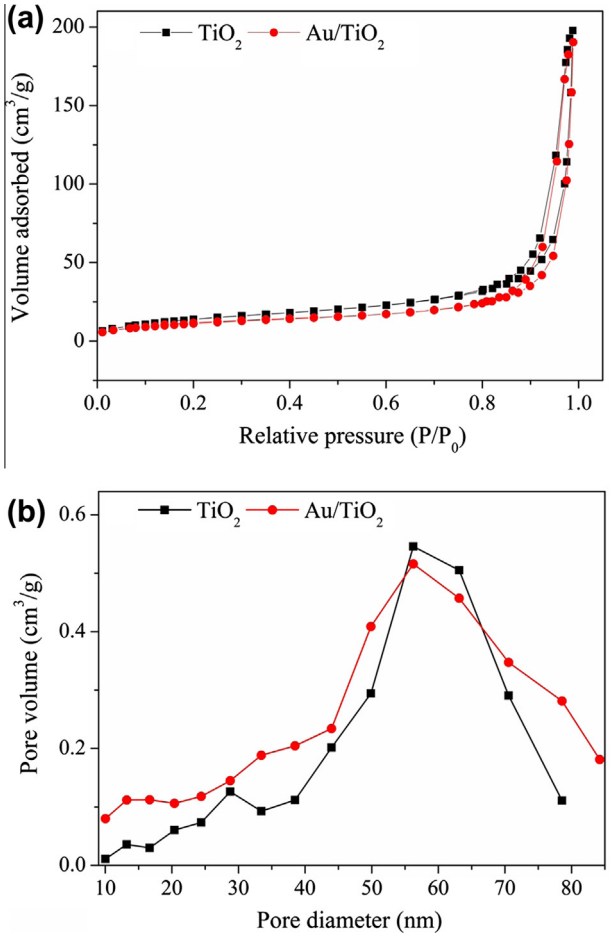

Fig. 4. (a) Nitrogen adsorption–desorption isotherms and (b) pore diameter distribution curves as determined using desorption data and the BJH model for TiO_2 films scratched off on FTO and gold coated FTO surfaces.

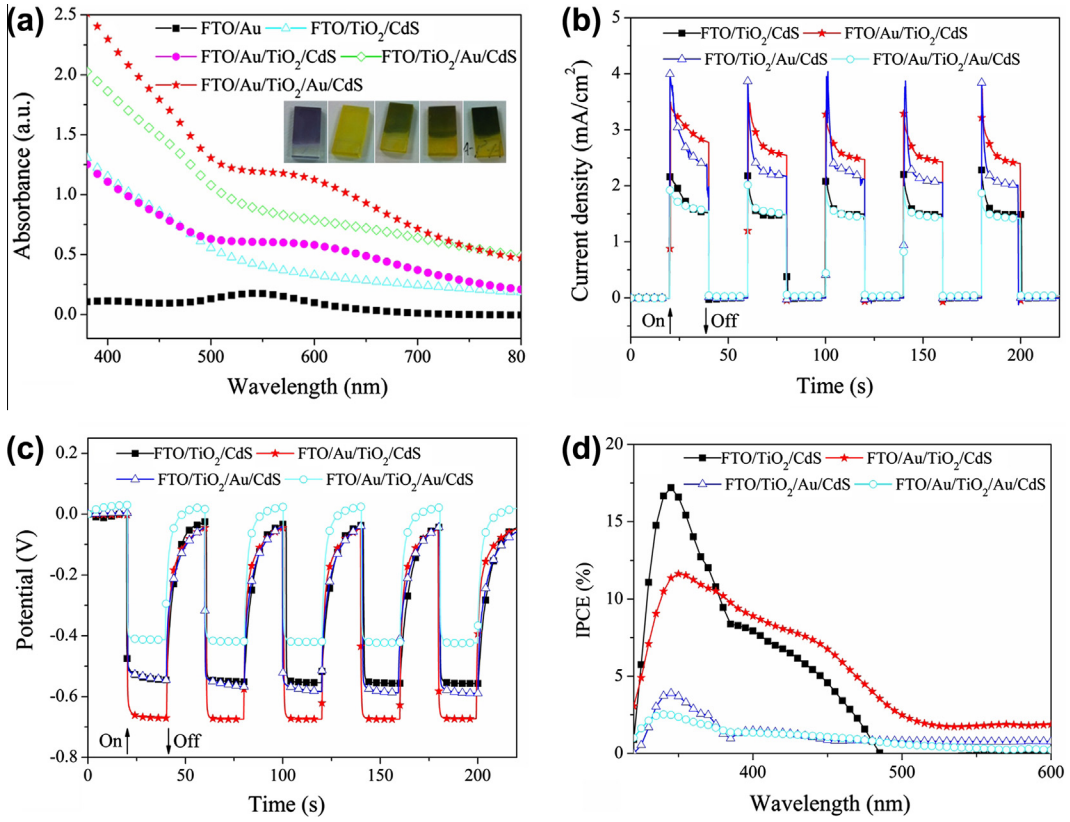

Fig. 5. (a) UV–vis absorption spectra and photographs, (b) photocurrent density, (c) open-circuit voltage and (d) IPCE of different hybrid samples. The number of SILAR cycles applied to deposit CdS was 5.

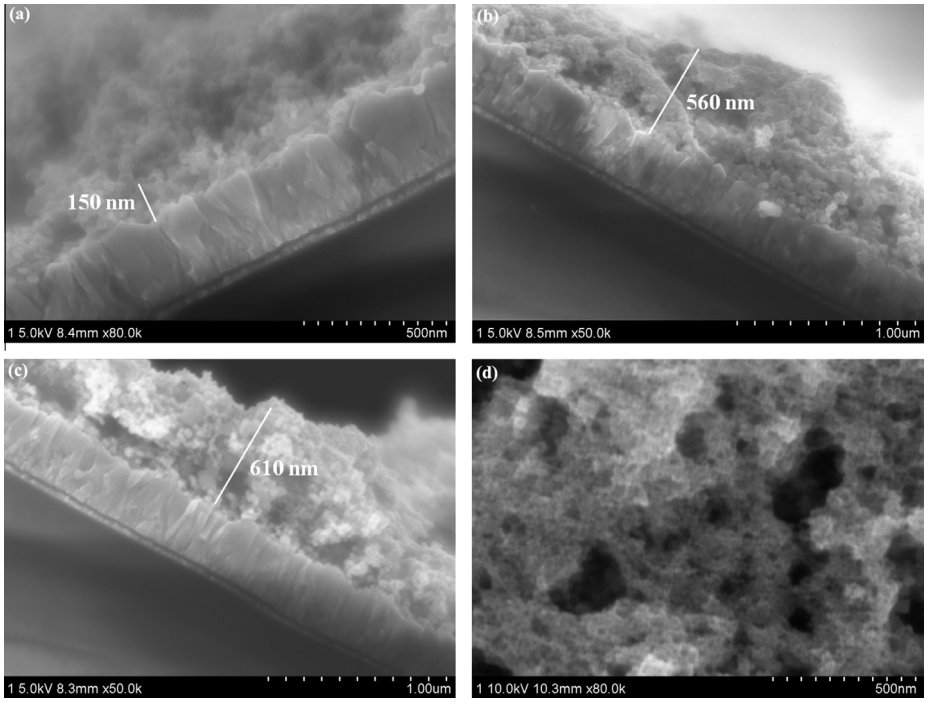

Fig. 6. (a)–(c) Cross section and (d) surface images of FTO/Au/TiO_2/CdS hybrids with the number of SILAR cycles applied to deposit CdS for (a) 1, (b) 7 and (c)–(d) 8, respectively.

from scattering effect [39] and near-field enhancement effect [40–42]. The light might be preferentially scattered and trapped into the hybrid film by multiple and high-angle scattering on the surface of gold NPs as sub-wavelength scattering elements, causing an increase of effective optical path length in the cell (Fig. 1a). Furthermore, plasmonic gold NPs with their effective dipole moment located close to the TiO_2 layer could favor the strong local field enhancement around the gold NPs and near-field coupling with

the TiO_2 semiconductor, increasing the absorption of semiconductor surrounding and cross-section [43,44]. Compared to the FTO/TiO_2/CdS and FTO/Au/TiO_2/CdS hybrids, the FTO/TiO_2/Au/CdS sample shows the absorption enhancement within a broad wave range. This indicates that the absorption enhancement should be attributed to the presence of gold films on the TiO_2 surface. For the FTO/Au/TiO_2/Au/CdS hybrid, the plasmonic-mediated absorption enhancement in the range from 500 nm to 700 nm is distinctly observed again, indicating the role of plasmonic gold below the porous TiO_2 film. Our result indicates that the gold below the porous TiO_2 film presents the SP effect.

Besides the improving light absorption induced by the plasmonic gold, the facilitating formation of electron–hole pairs in the near-surface region of semiconductor by the LSPR effect of metal NPs has been broadly reported [45–47], resulting in the enhancement of photocurrents [25,43,48]. Our results have confirmed the obvious enlargement of photocurrent and photovoltage signals for FTO/Au/TiO_2/CdS hybrid upon photoirradiation (Fig. 5b and c) by constructing a photoelectrochemical cell system with the platinum foil as a counter electrode and aqueous 0.2 M Na_2S as the electrolyte. The photocurrent densities in all hybrids are almost to be zero without photoillumination. The photogenerated electron–hole pairs are quickly produced upon photoillumination. The photogenerated electrons in the conduction band (CB) of CdS QDs are injected into the CB of TiO_2 NPs and then transported to the FTO substrate due to the energy difference between their band edges. The Na_2S in the solution gets the holes, resulting in the photocurrent in the circuit and open-circuit voltage. The shapes of photocurrent and open-circuit voltage curves keep consistent within five cycles, implying good stability of the hybrids. Compared to the FTO/TiO_2/CdS, the FTO/Au/TiO_2/CdS hybrid shows superior photoelectrochemical properties by introducing plasmonic gold NPs, which might improve the excited electron transport and suppress the charge recombination in the photoanode since the formation of a stepwise energy level between TiO_2 and FTO (Fig. 1b). This phenomenon has also been described by Shibata et al. [49]. The FTO/TiO_2/Au/CdS and FTO/Au/TiO_2/Au/CdS hybrids have lower photocurrent densities, which might be attributed to the trapping of photogenerated electrons in TiO_2 by gold NPs [24,50]. Fig. 5(d) displays the results of IPCE of different hybrids. The peak around 360 nm is attributed to the strong photoabsorption of TiO_2 NPs film. For the FTO/TiO_2/CdS film, the broad peak from 380 nm to 480 nm corresponds to the absorption of CdS QDs. In contrast, the FTO/Au/TiO_2/CdS film shows increased IPCE in the visible range due to the gold NPs primarily as light scattering centers [51]. The obvious decrease in the photocurrent and IPCE responses for FTO/TiO_2/Au/CdS and FTO/Au/TiO_2/Au/CdS hybrids might be attributed to the trap and capture of gold NPs to the photogenerated electrons [50]. Therefore, the plasmonic gold beneath TiO_2 enhances charge separation and transport and reduces charge recombination, which is in good agreement with results reported by others [51].

Furthermore, the amount of CdS QDs in QDSSCs is an important influencing factor to the photovoltaic performance [52,53]. Fig. 6 shows the surface and cross section SEM images of different hybrids. From the cross section images, we can clearly see that the thickness of CdS on the TiO_2 surface after one SILAR cycle is about 100 nm (Fig. 6a), which increases to 450 nm, 510 nm and 560 nm, respectively, after 5, 7 and 8 SILAR cycles (Figs. 3h, 6b and c). The CdS layer becomes densely with increasing the number of SILAR cycles for depositing CdS (Fig. 6d). CdS QDs tend to grow on the surface and inside of porous TiO_2 film. The UV–vis absorption

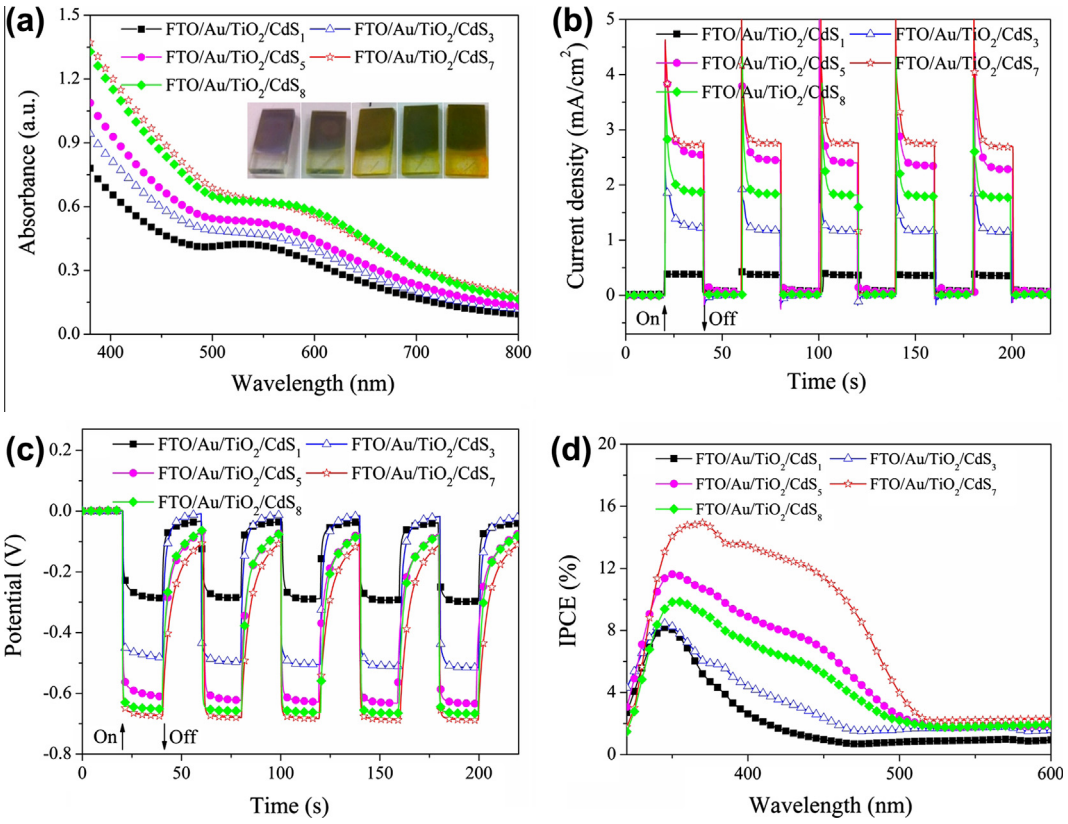

Fig. 7. (a) UV–vis absorption spectra and photographs, (b) photocurrent density, (c) open-circuit voltage and (d) IPCE of FTO/Au/TiO_2/CdS hybrids with different numbers of SILAR cycles applied to deposit CdS.

spectra of FTO/Au/TiO_2/CdS hybrids are enhanced by increasing the number of SILAR cycles from 1 to 7 (Fig. 7a) and remain stable after seven cycles due to most of the surface of porous TiO_2 film covered by the CdS crystallites, which hinders the further adsorption of Cd^{2+} and S^{2-} to form CdS. Furthermore, the absorbance spectra related to plasmon mode of gold in the range from 500 nm to 650 nm shows a redshift with the number increase of SILAR cycles. The absorption edge between 380 nm and 440 nm slightly shifts towards high wavelength with the increase in deposition cycles, indicating the growth of the CdS particles. Moreover, the increasing SILAR cycle also triggers a red shift of absorption spectrum [54], resulting in the decrease of optical bandgap related to the quantum size effect [55,56]. Besides, we observe an obvious increase in the photocurrent density and open-circuit potential with the number of SILAR cycle up to 7 as showed in Fig. 7(b) and (c). However, both parameters further decrease when the number of SILAR cycles rises up to 8. A high incorporated amount of CdS induced by more SILAR cycles might cause the conglomeration of CdS crystal nucleus and the limited diffusion of Na_2S into the FTO/Au/TiO_2/CdS hybrid electrode. The presence of thick absorber layers would thus impose a high barrier for electron tunneling and transferring [57,58] because electron tunneling probability exponentially decays with distance [59]. Fig. 7(d) shows the IPCE responses of different FTO/Au/TiO_2/CdS hybrids, which demonstrates the similar trend to the photocurrent density and open-circuit potential. This observation features the importance of the precise control over the architecture of photoanode in achieving the optimum performance via simple electrodeposition and SILAR processes. Since the performances of FTO/Au/TiO_2/CdS hybrids depend on the size, shape and interparticle spacing of plasmonic gold, and dielectric property of surrounding medium of gold, it is available to improve the photoelectric activity of the hybrids by designing and synthesizing targeted gold plasmons. Our further work will be carried out to prepare the adjustable gold plasmons by changing the parameters of gold electrodeposition to improve the photovoltaic performances of FTO/Au/TiO_2/CdS hybrids.

4. Conclusions

We develop CdS quantum dot (QD)-sensitized TiO_2 photoanodes with effectively enhanced photovoltaic performance by using plasmonic gold nanocrystals as light concentrators. The light scattering and trapping of plasmonic gold nanostructures and the near-field coupling of plasmonic gold with the TiO_2 and CdS semiconductors increase the effective path length of incident light in absorber layer and the absorption of semiconductor surrounding and cross-section. The gold plasmons also facilitate electron extraction in TiO_2 and CdS semiconductors, and an optimized Au/TiO_2/CdS structure shows the predominance in transporting the photogenerated electrons toward the electrode surface to inhibit charge recombination as evidenced increase in photocurrent, open-circuit voltage and incident photon-to-current conversion efficiency. The plasmonic light-trapping concept favors new designs for quantum dots-sensitized film solar cells and related energy conversion devices.

Acknowledgements

This work was supported by the National Natural Science Foundation of China (51272237, 61205158 and 51172208), the Visiting Scholars Fund of State Key Lab of Silicon Materials, Zhejiang University (SKL2011-20), the Qianjiang Talent Program of Zhejiang Province (QJD1102007), the China Postdoctoral Science Foundation (Nos. 2012M520063, 2013T60587 and Bsh1201016), the 521 Talent Project of Zhejiang Sci-Tech University, the Scientific Research Foundation for the Returned Overseas Chinese Scholars (State Education Ministry) and the Technology Foundation for Selected Overseas Chinese Scholar of China.

References

[1] B. O'Regan, M. Gratzel, Nature 353 (1991) 737–740.
[2] X.J. Liu, L.K. Pan, T. Lv, Z. Sun, J. Alloys Comp. 583 (2014) 390–395.
[3] G.Z. Wu, Y. Shen, Q.H. Wu, F. Gu, M. Cao, L.J. Wang, J. Alloys Comp. 551 (2013) 176–179.
[4] T. Shu, Z.L. Ku, J. Alloys Comp. 586 (2014) 257–260.
[5] Y. Chen, Y.H. Tang, S.L. Luo, C.B. Liu, Y. Li, J. Alloys Comp. 578 (2013) 242–248.
[6] G.L. Zhao, H. Kozuka, T. Yoko, Sol. Energy Mater. Sol. Cells 46 (1997) 219–231.
[7] L.M. Peter, D.J. Riley, E.J. Tull, K.G.U. Wijayantha, Chem. Commun. 10 (2002) 1030–1031.
[8] K.G.U. Wijayantha, L.M. Peter, L.C. Otley, Sol. Energy Mater. Sol. Cells 83 (2004) 263–271.
[9] L.J. Kong, J.M. Li, G.L. Chen, C.F. Zhu, W.F. Liu, J. Alloys Comp. 573 (2013) 112–117.
[10] I. Robel, V. Subramanian, M. Kuno, P.V. Kamat, J. Am. Chem. Soc. 128 (2006) 2385–2393.
[11] R. Plass, P. Serge, J. Krueger, M. Gratzel, J. Phys. Chem. B 106 (2002) 7578–7580.
[12] R.D. Schaller, V.I. Klimov, Phys. Rev. Lett. 92 (2004) 186601.
[13] J.L. Blackburn, D.C. Selmarten, R.J. Ellingson, M. Jones, O. Micic, A.J. Nozik, J. Phys. Chem. B 109 (2005) 2625–2631.
[14] J.H. Bang, P.V. Kamat, Adv. Funct. Mater. 20 (2010) 1970–1976.
[15] S.Y. Yang, A.S. Nair, R. Jose, S. Ramakrishna, Energy Environ. Sci. 3 (2010) 2010–2014.
[16] W.L. Barnes, A. Dereux, T.W. Ebbesen, Nature 424 (2003) 824–830.
[17] T. Singh, D.K. Pandya, R. Singh, J. Alloys Comp. 552 (2013) 294–298.
[18] Z.H. Chen, Y.B. Tang, C.P. Liu, Y.H. Leung, G.D. Yuan, L.M. Chen, Y.Q. Wang, I. Bello, J.A. Zapien, W.J. Zhang, C.S. Lee, S.T. Lee, J. Phys. Chem. C 113 (2009) 13433–13437.
[19] D. Derkacs, S.H. Lim, P. Matheu, W. Mar, E.T. Yu, Appl. Phys. Lett. 89 (2006) 093103.
[20] S. Pillai, K.R. Catchpole, T. Trupke, M.A. Green, J. Appl. Phys. 101 (2007) 093105.
[21] K.R. Catchpoleand, A. Polman, Appl. Phys. Lett. 93 (2008) 191113.
[22] W. Smith, S. Mao, G.H. Lu, A. Catlett, J.H. Chen, Y.P. Zhao, Chem. Phys. Lett. 485 (2010) 171–175.
[23] J.Z. Zhang, C. Noguez, Plasmonics 3 (2008) 127–150.
[24] L.P. Liu, G.M. Wang, Y. Li, Y.D. Li, J.Z. Zhang, Nano Res. 4 (2011) 249–258.
[25] Y. Nishijima, K. Ueno, Y. Yokota, K. Murakoshi, H. Misawa, J. Phys. Chem. Lett. 1 (2010) 2031–2036.
[26] K.L. Kelly, E. Coronado, L.L. Zhao, G.C. Schatz, J. Phys. Chem. B 107 (2003) 668–677.
[27] X.H. Li, W.C.H. Choy, L.J. Huo, F.X. Xie, W.E.I. Sha, B.F. Ding, X. Guo, Y.F. Li, J.H. Hou, J.B. You, Y. Yang, Adv. Mater. 24 (2012) 3046–3052.
[28] A.P. Liu, T. Xu, Q.H. Ren, M. Yuan, W.J. Dong, W.H. Tang, Electrochem. Commun. 25 (2012) 74–78.
[29] U. Dogan, M. Kaya, A. Cihaner, M. Volkan, Electrochim. Acta 85 (2012) 220–227.
[30] J.X. Fang, H.J. You, B.J. Ding, X.P. Song, Electrochem. Commun. 9 (2007) 2423–2427.
[31] C.H. Chang, Y.L. Lee, Appl. Phys. Lett. 91 (2007) 053503.
[32] C.F. Chi, Y.L. Lee, H.S. Weng, Nanotechnology 19 (2008) 125704.
[33] Y. Tian, T. Tatsuma, J. Am. Chem. Soc. 127 (2005) 7632–7637.
[34] L. Cheng, A.P. Liu, S. Peng, H.W. Duan, ACS Nano 4 (2010) 6098–6104.
[35] B.M. Reinhard, M. Siu, H. Agarwal, A.P. Alivisatos, J. Liphardt, Nano Lett. 5 (2005) 2246–2252.
[36] P. Reineck, G.P. Lee, D. Brick, M. Karg, P. Mulvaney, U. Bach, Adv. Mater. 24 (2012) 4750–4755.
[37] E. Kazuma, N. Sakai, T. Tatsuma, Chem. Commun. 47 (2011) 5777–5779.
[38] M. Heo, H. Cho, J.W. Jung, J.R. Jeong, S. Park, J.Y. Kim, Adv. Mater. 23 (2011) 5689–5693.
[39] D.M. Schaadt, B. Feng, E.T. Yu, Appl. Phys. Lett. 86 (2005) 063106.
[40] A.J. Morfa, K.L. Rowlen, T.H. Reilly, M.J. Romero, J. van de Lagemaat, Appl. Phys. Lett. 92 (2008) 013504.
[41] S.S. Kim, S.I. Na, J. Jo, D.Y. Kim, Y.C. Nah, Appl. Phys. Lett. 93 (2008) 073307.
[42] J.L. Wu, F.C. Chen, Y.S. Hsiao, F.C. Chien, P.L. Chen, C.H. Kuo, M.H. Huang, C.S. Hsu, ACS Nano 5 (2011) 959–967.
[43] R. Bukasov, T.A. Ali, P. Nordlander, J.S. Shumaker-Parry, ACS Nano 4 (2010) 6639–6650.
[44] J.F. Zhu, M. Xue, H.J. Shen, Z. Wu, S. Kim, J.J. Ho, A. Hassani-Afshar, B.Q. Zeng, K.L. Wang, Appl. Phys. Lett. 98 (2011) 151110.
[45] D.B. Ingram, S. Linic, J. Am. Chem. Soc. 133 (2011) 5202–5205.
[46] K. Awazu, M. Fujimaki, C. Rockstuhl, J. Tominaga, H. Murakami, Y. Ohki, N. Yoshida, T. Watanabe, J. Am. Chem. Soc. 130 (2008) 1676–1680.
[47] E. Thimsen, F. Le Formal, M. Gratzel, S.C. Warren, Nano Lett. 11 (2011) 35–43.
[48] D. Pacifici, H.J. Lezec, H.A. Atwater, Nat. Photonics 1 (2007) 402–406.
[49] N. Shibata, A. Goto, K. Matsunaga, T. Mizoguchi, S.D. Findlay, T. Yamamoto, Y. Ikuhara, Phys. Rev. Lett. 102 (2009) 136105.
[50] V. Subramanian, E. Wolf, P.V. Kamat, J. Phys. Chem. B 105 (2001) 11439–11446.

[51] I. Zarazua, E. De la Rosa, T. Lopez-Luke, J. Reyes-Gomez, S. Ruiz, C.A. Chavez, J.Z. Zhang, J. Phys. Chem. C 115 (2011) 23209–23220.
[52] Y.J. Tak, S.J. Hong, J.S. Lee, K.J. Yong, J. Mater. Chem. 19 (2009) 5945–5951.
[53] Y.L. Lee, C.H. Chang, J. Power Sources 185 (2008) 584–588.
[54] Y.H. Zhang, J. Zhu, X.C. Yu, J.F. Wei, L.H. Hu, S.Y. Dai, Solar Energy 86 (2012) 964–971.
[55] V. Senthamilselvi, K. Ravichandran, K. Saravanakumar, J. Phys. Chem. Solids 74 (2013) 65–69.
[56] C.L. Cao, C.G. Hua, W.D. Shen, S.X. Wang, Y.S. Tian, X. Wang, J. Alloys Comp. 523 (2012) 139–145.
[57] H. Chen, W.Y. Fu, H.B. Yang, P. Sun, Y.Y. Zhang, L.R. Wang, W.Y. Zhao, X.M. Zhou, H. Zhao, Q. Jing, X.F. Qi, Y.X. Li, Electrochim. Acta 56 (2010) 919–924.
[58] L.W. Chong, H.T. Chien, Y.L. Lee, J. Power Sources 195 (2010) 5109–5113.
[59] M. Kondon, J. Kim, N. Udawatte, D. Lee, J. Phys. Chem. C 112 (2008) 6695–6699.